Mon. Not. R. Astron. Soc. **296,** 275–286 (1998)

Gamma-ray bursts from internal shocks in a relativistic wind: temporal and spectral properties

F. Daigne and R. Mochkovitch
Institut d'Astrophysique de Paris, CNRS, 98 bis Boulevard Arago, 75014 Paris, France

Accepted 1997 November 5. Received 1997 October 27; in original form 1997 July 17

ABSTRACT

We construct models for gamma-ray bursts in which the emission comes from internal shocks in a relativistic wind with a highly non-uniform distribution of the Lorentz factor. We follow the evolution of the wind using a very simplified approach in which a large number of layers interact by direct collisions but all pressure waves have been suppressed. We suppose that the magnetic field and the electron Lorentz factor reach large equipartition values in the shocks. Synchrotron photons emitted by the relativistic electrons have a typical energy in the gamma-ray range in the observer frame. Synthetic bursts are constructed as the sum of the contributions from all the internal elementary shocks, and their temporal and spectral properties are compared with the observations. We reproduce the diversity of burst profiles, the 'FRED' shape of individual pulses and the short time-scale variability. Synthetic bursts also satisfy the duration–hardness relation and individual pulses are found to be narrower at high energy, in agreement with the observations. These results suggest that internal shocks in a relativistic wind may indeed be at the origin of gamma-ray bursts. A potential problem, however, is the relatively low efficiency of the dissipation process. If the relativistic wind is powered by accretion from a disc to a stellar mass black hole, it implies that a substantial fraction of the available energy is injected into the wind.

Key words: accretion, accretion discs – radiation mechanisms: non-thermal – shock waves – gamma-rays: bursts.

1 INTRODUCTION

Since 1991 the BATSE experiment on board the *Compton Gamma-Ray Observatory* satellite has observed more than 1800 gamma-ray bursts (hereafter GRBs). The burst distribution is isotropic over the sky but non-homogeneous in distance (Fishman & Meegan 1995 and references therein) which has been regarded as a strong indication that GRBs lie at cosmological distances (Paczyński 1991). However, the possibility that GRBs belong to a large galactic halo (Hartmann et al. 1994) could not be excluded a priori. This long standing controversy (see Nemiroff et al. 1995) about the burst distance scale may finally be solved by the recent observations of transient optical counterparts for two GRBs. In the case of GRB 970228 (van Paradijs et al. 1997; Sahu et al. 1997a) the point-like counterpart appears to be associated with an extended source which is probably a distant galaxy. The case of GRB 970508 is even more spectacular, since the spectrum of the counterpart shows Fe II and Mg II lines due to absorbers on the line of sight at a redshift $z = 0.835$ (Metzger et al. 1997). If the association of the visible source with the burst is confirmed, GRB 970508 must be a very distant object at $z \geq 0.835$. If GRBs are placed at cosmological distances the $\log N$–$\log P$ (peak flux) curve and the value of $< V/V_{\max} >$ can be naturally interpreted in terms of cosmological effects, and indicate that GRBs have typical redshifts in the range 0.3 – 1 (Piran 1992; Mao & Paczyński 1992; Fenimore et al. 1993).

Modelling GRBs is a difficult task due to the extreme diversity of burst profiles, the non-thermal spectra and the lack of a clear signature for the emission processes involved. Most cosmological models, however, share some common characteristics. The source, which must be able to release (between 10 keV and 10 MeV) an energy $E_\gamma \gtrsim 10^{51}/4\pi$ erg sr^{-1} on a time-scale of seconds, is generally supposed to be a stellar-mass black hole accreting material from a disc. Such a configuration can result from the coalescence of two neutron stars (Eichler et al. 1989; Paczyński 1991; Narayan, Paczyński & Piran 1992), the disruption of the neutron star in a neutron star–black hole binary (Narayan et al. 1992; Mochkovitch et al. 1993) or the collapse of a massive star (Woosley 1993). The power emitted by cosmological GRBs is orders of magnitude larger than the Eddington luminosity and cannot come directly from the disc surface. The released energy instead drives a wind which has to become relativistic both to produce gamma-rays and to avoid photon–photon annihilation along the line of sight (Baring 1995; Sari & Piran 1997a). The Lorentz factor Γ must reach values of 10^2–10^3 which limits the allowed amount of baryonic pollution in the flow to a very low level. A few mechanisms which could possibly achieve such a severe constraint have been proposed: (i)

a magnetically driven outflow originating from the disc or powered by the Blandford–Znajek (1977) effect (Thompson 1994; Mészáros & Rees 1997a); (ii) reconnection of magnetic field lines in the disc corona (Narayan et al. 1992); or (iii) neutrino–antineutrino annihilation in a funnel along the rotation axis of the system (Mészáros & Rees 1992; Mochkovitch et al. 1993, 1995). It is supposed in (i) and (ii) that the field has reached huge values $B \gtrsim 10^{15}$ G. Concerning (iii) Ruffert et al. (1997) have shown recently that $\nu\bar{\nu}$ annihilation does not provide enough energy to account for cosmological GRBs except perhaps for very massive discs, e.g. those which could result from the collapse of a massive star.

The energy initially stored in kinetic form within the relativistic wind must then be converted into gamma-rays. This can be done during the deceleration of the wind resulting from its interaction with the interstellar medium (Rees & Mészáros 1992; Mészáros & Rees 1993) or with a dense radiation field (Shemi 1994). In the first case the emission comes from electrons accelerated in the forward and reverse shocks which then radiate synchrotron and inverse Compton photons in a magnetic field frozen in the wind, or which has come to equipartition with the shocked material (Mészáros, Laguna & Rees 1993). In the second case, photons of the ambient radiation field (in the central regions of globular clusters or active galactic nuclei) interact with the electrons (Shemi 1994; Shaviv & Dar 1995) or ions (Shaviv & Dar 1996) of the wind and undergo a boost in energy by a factor Γ^2. With $\Gamma \lesssim 10^3$, optical photons can be shifted to the gamma-ray range. In these two models the duration of the burst is $t_b \sim r_{dec}/c\Gamma^2$ where r_{dec} is the deceleration radius of the wind.

Another possibility suggested by Rees & Mészáros (1994) supposes that the Lorentz factor in the wind is variable so that successive shells can have large relative velocities leading to the formation of internal shocks. The energy which is dissipated in these shocks can then be radiated as gamma-rays via the production of pions in proton–proton collisions (Paczyński & Xu 1994) or by synchrotron (or inverse Compton) emission of accelerated electrons. There are several important differences between the deceleration and internal shock models. In deceleration models, the duration and time profile of the burst depend on Γ, on the value of the deceleration radius and on the structure of the emitting shell. In internal shock models, the duration of the burst is directly related to the duration of energy injection at the source, and the time profile is essentially determined by the variations of the Lorentz factor (Sari & Piran 1997a; Kobayashi, Piran & Sani 1997).

Burst profiles and spectra have already been obtained (sometimes in a rather detailed manner) in the case of deceleration models (Fenimore, Madras & Nayakshin 1997; Panaitescu et al. 1997; Panaitescu & Mészáros 1997), and the purpose of this work is to present the same kind of quantitative analysis for internal shock models. In Section 2 we describe our method of following the evolution of the relativistic wind and we discuss the emission processes; Sections 3 and 4, respectively, deal with the temporal and spectral properties of our synthetic burst models and in Section 5 we present our conclusions.

2 A SIMPLE MODEL OF THE RELATIVISTIC WIND

2.1 Description of the model

We do not discuss in this paper the nature of the source (coalescence of two neutron stars, neutron star–black hole binary, collapse of a massive star or something else) which is initially responsible for the energy release. We also suppose that a relativistic wind carrying the energy has emerged from the source, with an average Lorentz factor $\bar{\Gamma}$ of a few hundreds.

To study the evolution of the relativistic wind, we have developed a very simple model in which a succession of layers is emitted every 2 ms with a varying Lorentz factor, during a total time t_w. The mass of the layers is proportional to $1/\Gamma$ so that the energy injection rate is constant. We follow the layers as the wind expands and when a rapid layer (of mass m_1 and Lorentz factor Γ_1) catches up with a slower one (m_2, $\Gamma_2 < \Gamma_1$) they collide and merge to form a single shell of resulting Lorentz factor Γ_r. If the dissipated energy

$$e = m_1c^2\Gamma_1 + m_2c^2\Gamma_2 - (m_1 + m_2)c^2\Gamma_r, \tag{1}$$

can be radiated in the gamma-ray range on a time-scale shorter than the shell expansion time (in the comoving frame)

$$t_{ex} \simeq \frac{r}{c\Gamma_r}, \tag{2}$$

where r is the shell radius, the burst profile will be made by a succession of elementary contributions of duration (in the observer frame)

$$\Delta t \simeq \frac{r}{2c\Gamma_r^2}. \tag{3}$$

We estimate Γ_r by considering that most of the energy available in the collision has been already released when the less massive of the two layers has swept up a mass comparable to its own mass in the other layer (internal shocks being only mildly relativistic). Then

$$\Gamma_r \simeq \sqrt{\Gamma_1\Gamma_2}, \tag{4}$$

and

$$e = mc^2(\Gamma_1 + \Gamma_2 - 2\Gamma_r), \qquad m = \min(m_1, m_2). \tag{5}$$

After the complete redistribution of momentum and energy, the Lorentz factor of the merged layer finally becomes

$$\Gamma_f = \sqrt{\Gamma_1\Gamma_2\frac{m_1\Gamma_1 + m_2\Gamma_2}{m_1\Gamma_2 + m_2\Gamma_1}}. \tag{6}$$

Two more conditions have to be satisfied for an elementary shock to be produced and observed: (i) the two layers must collide at a relative velocity larger than the local sound speed and (ii) the wind must be transparent to the emitted photons. The relative velocity of the two layers is given by

$$\frac{v_{rel}}{c} \simeq \frac{\Gamma_1^2 - \Gamma_2^2}{\Gamma_1^2 + \Gamma_2^2}, \tag{7}$$

with $\Gamma_1 > \Gamma_2$ and $\Gamma_{1,2} \gg 1$. We have adopted a sound speed $v_s/c = 0.1$ but we have checked that other choices make little difference in the results since the main contribution to the burst comes from shocks corresponding to large differences of the Lorentz factor $\Gamma_1/\Gamma_2 \gtrsim 2$.

The transparency of the wind to the emitted photons has been computed in the following way: in each collision between layers, a 'photon shell' is generated which then catches up with all the layers ahead of it. It travels through a total optical depth

$$\tau = \kappa_T \sum_{i>i_m} \frac{m_i}{4\pi r_i^2}, \tag{8}$$

where κ_T is the Thomson opacity and r_i the radius of layer i when it is reached by the photon shell. The sum is over all indices i larger than i_m, which corresponds to the two merged layers. For the average Lorentz factor $\bar{\Gamma} \gtrsim 100$ used here, it appears that the wind is transparent to the emitted photons except for a few early collisions.

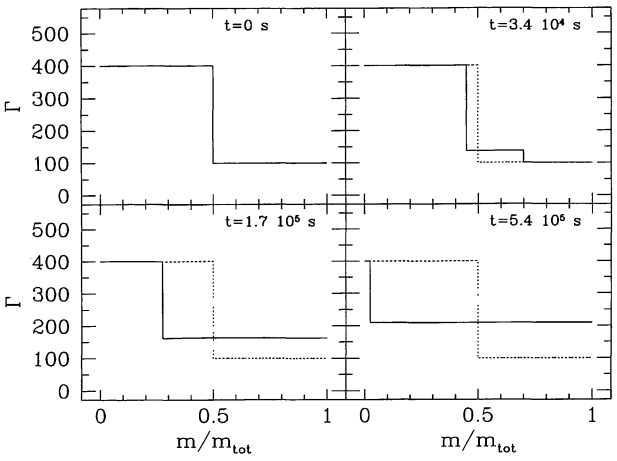

Figure 1. Distribution of the Lorentz factor in the wind at different times in Lagrangian coordinates $m/m_{\rm tot}$ ($m_{\rm tot}$ being the total mass of the wind). The initial distribution ($t = 0$) consists of 5000 layers with $\Gamma = 100$ in the 1000 first emitted layers and $\Gamma = 400$ in the rest of the wind. Since the mass of the layers is proportional to $1/\Gamma$ the slow and rapid parts contain an equal mass. At $t = 3.4 \times 10^4$ s, a forward and a reverse shock are propagating into the wind. In our simple model they are located on a single Eulerian shell of increasing mass. At $t = 1.7 \times 10^5$ s the forward shock has already crossed the whole slow part, and at $t = 5.4 \times 10^5$ s the reverse shock reaches the end of the rapid part. The dashed line shows the initial distribution of the Lorentz factor.

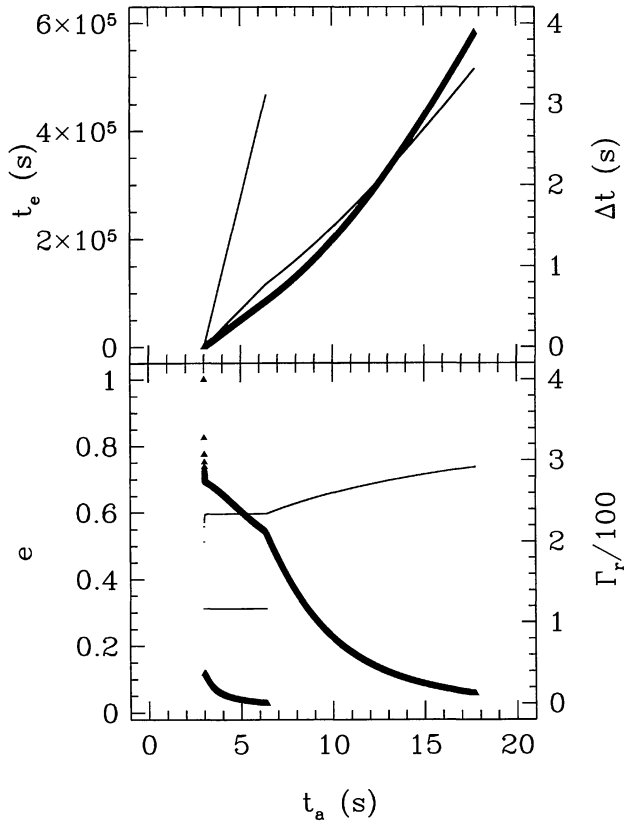

Figure 2. Physical parameters of the elementary shocks. Upper panel: (thick line) emission time $t_{\rm e}$ and (thin line) duration Δt of the signal (in the observer frame) both as a function of arrival time $t_{\rm a}$. Lower panel: (thick line) energy e dissipated in the shock in arbitrary units and (thin line) Lorentz factor $\Gamma_{\rm r}$ at the shock location.

The arrival time of each of the elementary contributions from internal shocks is calculated relative to a signal which would have travelled at the speed of light from the source to the observer. It is given by

$$t_{\rm a} = t_{\rm e} - \frac{r}{c}, \tag{9}$$

where $t_{\rm e}$ is the emission time and r the distance to the source of the two merged layers. The evolution of the system is followed until all the layers are ordered with Γ decreasing from the front to the back of the wind. The efficiency of the dissipation process can then be obtained as

$$f_{\rm d} = \frac{\sum_s e_s}{\sum_i m_i c^2 \Gamma_i}, \tag{10}$$

where the e_s are the energies released in each of the internal elementary shocks and the m_i, Γ_i are the initial masses and Lorentz factors of the layers.

This very simple approach is naturally very crude because it neglects all pressure waves propagating throughout the layers. Nevertheless, we expect that it can still capture the basic features of the real process. As a first example we have represented in Fig. 1 the evolution of the Lorentz factor at different times, when the initial distribution of Γ consists of 5000 layers (i.e. $t_{\rm w} = 10$ s) with $\Gamma(n) = 400$ for $n = 1$ to 4000 and $\Gamma(n) = 100$ for $n = 4001$ to 5000 ($n = 1$ for the last emitted layer). Such a wind is then divided between a 'slow' part which is emitted first and a rapid part which will progressively collide against the slow part. The total masses injected in the slow and rapid parts are equal. After the first collision has occurred, a separation layer of increasing mass is formed between the slow and rapid parts. We have plotted in Fig. 2 the values of $t_{\rm e}$, $\Gamma_{\rm r}$, Δt and e for the elementary shocks as a function of arrival time $t_{\rm a}$. The evolution of the shell system is essentially completed after a time $t_{\rm e} \sim t_{\rm var}\bar{\Gamma}^2$, where $t_{\rm var}$ is the characteristic time-scale for the variations of the Lorentz factor. As expected, the plots of $\Gamma_{\rm r}$, Δt and e have two branches, corresponding to collisions taking place on both sides of the separation layer. They mimic the forward and reverse shocks which, in our simple model, are located on a single surface.

The efficiency $f_{\rm d}$ of the dissipation process is rather low, 10 per cent in this specific case, typically less than 15 per cent. This is a severe problem, which can become even worse if only a fraction of the dissipated energy is radiated in the gamma-ray range. This issue is examined in the next section.

2.2 Emission processes

The process by which the dissipated energy is finally radiated depends on the energy distribution of protons and electrons in the shocked material and on the values of the comoving density and magnetic field. The average energy which is dissipated per proton in a shock between two layers of equal mass is given by

$$\epsilon = (\Gamma_{\rm int} - 1) m_{\rm p} c^2$$
$$\text{with} \quad \Gamma_{\rm int} = \frac{1}{2}\left[\left(\frac{\Gamma_1}{\Gamma_2}\right)^{1/2} + \left(\frac{\Gamma_2}{\Gamma_1}\right)^{1/2}\right], \tag{11}$$

where $\Gamma_{\rm int}$ is the Lorentz factor for internal motions in the shocked material. With $\Gamma_1/\Gamma_2 = 4$, which corresponds to a mildly relativistic shock ($v_{\rm rel}/c = 0.88$), $\epsilon \gtrsim 200$ MeV.

A mechanism which could directly extract the energy from the protons has been proposed by Paczyński & Xu (1994) since the value of ϵ is large enough for the production of pions in pp

collisions. The pions then decay with the emission of gamma-rays. The global efficiency of this mechanism is low, of the order of 10^{-3} for $\Gamma_1/\Gamma_2 = 4$.

Another possibility, considered by Rees & Mészáros (1994), Papathanassiou & Mészáros (1996) and Sari & Piran (1997a), consists of supposing that the electrons have come into (at least partial) equipartition with the protons. If a fraction α_e of the dissipated energy goes to the electrons their characteristic Lorentz factor will be

$$\Gamma_e \simeq \alpha_e \frac{\epsilon}{m_e c^2}, \tag{12}$$

which, for $\alpha_e = 1/3$ (corresponding to a complete equipartition between protons, electrons and the magnetic field) and $\Gamma_1/\Gamma_2 = 4$ yields $\Gamma_e \sim 150$. The equipartition magnetic field is given by

$$B_{eq} \simeq \left(8\pi\alpha_B n\epsilon\right)^{1/2}, \tag{13}$$

where $\alpha_B \lesssim 1$ and n is the comoving proton number density

$$n \simeq \frac{\dot{M}}{4\pi r^2 \bar{\Gamma} m_p c} \simeq \frac{\dot{E}}{4\pi r^2 \bar{\Gamma}^2 m_p c^3}. \tag{14}$$

Assuming $\dot{E} = 10^{52}$ erg.s^{-1}, $\bar{\Gamma} = 300$, $t_{var} = 1$ s and $\alpha_B = 1/3$ the equipartition magnetic field at a radius $r \sim ct_{var}\bar{\Gamma}^2$ where most of the collisions take place is $B_{eq} \sim (10^2 - 10^3)$ G depending on the ratio Γ_1/Γ_2.

Synchrotron emission by the accelerated electrons in the magnetic field occurs at a typical energy (in the observer frame)

$$E_{syn} = 50\left(\frac{\Gamma_r}{300}\right)\left(\frac{B}{1000\,\mathrm{G}}\right)\left(\frac{\Gamma_e}{100}\right)^2 \ \mathrm{eV}, \tag{15}$$

which corresponds to the UV range for $\Gamma_e = 100$. Gamma-rays can be produced by inverse Compton scattering on the synchrotron photons. Then

$$E_{IC} \simeq E_{syn}\Gamma_e^2 = 500\left(\frac{\Gamma_r}{300}\right)\left(\frac{B}{1000\,\mathrm{G}}\right)\left(\frac{\Gamma_e}{100}\right)^4 \ \mathrm{keV}, \tag{16}$$

and the fraction of the total power which is radiated by the inverse Compton process is

$$\alpha_{IC} = \frac{\tau_\star \Gamma_e^2}{1 + \tau_\star \Gamma_e^2}, \tag{17}$$

where

$$\tau_\star = \frac{\kappa_T M_\star}{4\pi r_\star^2} \tag{18}$$

is the optical depth of the shell of mass $M_\star$ and radius $r_\star$ which contains the relativistic electrons. An estimate of $M_\star$ is

$$M_\star = \frac{t_{syn}}{1 + \tau_\star \Gamma_e^2}\dot{M}_{shock}, \tag{19}$$

where

$$t_{syn} = 6\left(\frac{\Gamma_e}{100}\right)^{-1}\left(\frac{B}{1000\,\mathrm{G}}\right)^{-2} \ \mathrm{s} \tag{20}$$

is the synchrotron time of the relativistic electrons and $\dot{M}_{shock}$ the mass flow rate across the shock, both in the comoving frame of the shocked material. Since the shock moves with a Lorentz factor $\Gamma_s \simeq \bar{\Gamma}$, $\dot{M}_{shock}$ can be approximated by

$$\dot{M}_{shock} \simeq \frac{\dot{M}}{\bar{\Gamma}}. \tag{21}$$

From (18), (19) and (21) we obtain an implicit expression for $\tau_\star \Gamma_e^2$,

$$\tau_\star \Gamma_e^2 = \frac{\kappa_T \dot{M}_{shock} t_{syn} \Gamma_e^2}{4\pi r_\star^2 (1 + \tau_\star \Gamma_e^2)}. \tag{22}$$

With $r_\star \sim ct_{var}\bar{\Gamma}^2$, relations (20) and (21) for t_{syn} and $\dot{M}_{shock}$, (13) and (14) for B_{eq} and n, equation (22) gives (for $\kappa_T = 0.2$ cm^2 g^{-1})

$$\tau_\star \Gamma_e^2 (1 + \tau_\star \Gamma_e^2) \simeq 0.3 \frac{\alpha_e}{\alpha_B}, \tag{23}$$

which, for $\alpha_e \sim \alpha_B$ yields $\tau_\star \Gamma_e^2 \simeq 0.24$ and $\alpha_{IC} \simeq 0.19$. A larger fraction of the dissipated energy can be converted to gamma-rays if the magnetic field does not reach equipartition. With, for example, $\alpha_e/\alpha_B = 100$, $\tau_\star \Gamma_e^2$ rises to 5 and α_{IC} to 0.83. Smaller values of α_B could still increase α_{IC} but the energy of the inverse Compton photons would then become too small.

Conversely, if the electron Lorentz factor is large enough, gamma-rays can be directly produced by synchrotron emission. This will be the case if, instead of (12), one uses the expression of Γ_e given by Bykov & Mészáros (1996) who consider the scattering of electrons by turbulent magnetic field fluctuations. They get

$$\Gamma_e \sim \left[\left(\frac{\alpha_M}{\zeta}\right)\left(\frac{\epsilon}{m_e c^2}\right)\right]^{1/(3-\mu)}, \tag{24}$$

where α_M is the fraction of the dissipated energy which goes into magnetic fluctuations, ζ the fraction of the electrons which are accelerated and μ the index of the fluctuation spectrum. With $1.5 \leq \mu \leq 2$, $\alpha_M = 0.1 - 1$, $\zeta \sim 10^{-3}$ and $\epsilon/m_e c^2 \sim 500$ (for $\Gamma_1/\Gamma_2 = 4$) values of Γ_e in the range 10^3–10^4 can be obtained.

A fraction of the synchrotron photons will be shifted to even higher energy by inverse Compton scattering which now occurs in the limit where

$$w = \frac{\Gamma_e E_{syn}^0}{m_e c^2} \simeq 33\left(\frac{B}{1000\,\mathrm{G}}\right)\left(\frac{\Gamma_e}{10^4}\right)^3 \tag{25}$$

is large, $E_{syn}^0 = E_{syn}/\Gamma_r$ being the synchrotron energy in the comoving frame. The inverse Compton photons have an energy

$$E_{IC}^0 \simeq \Gamma_e m_e c^2 = 5\left(\frac{\Gamma_e}{10^4}\right) \ \mathrm{GeV} \tag{26}$$

in the comoving frame and carry a fraction

$$\alpha_{IC} = \frac{\tau_\star \Gamma_e^2 / w}{1 + \tau_\star \Gamma_e^2 / w} \tag{27}$$

of the dissipated energy. The optical depth $\tau_\star$ has to be computed with the Klein–Nishina cross-section which, in the limit $w \gg 1$, gives

$$\tau_\star \simeq \left[\frac{\kappa_T \dot{M}_{shock} t_{syn}}{4\pi r_\star^2 (1 + \tau_\star \Gamma_e^2/w)}\right]\left(\frac{3}{8w}\right)[1 + \ln(2w)], \tag{28}$$

and therefore

$$\frac{\tau_\star \Gamma_e^2}{w}\left(1 + \frac{\tau_\star \Gamma_e^2}{w}\right) \simeq 8\ 10^{-4}[1 + \ln(2w)]\left(\frac{\dot{E}}{10^{52}\ \mathrm{erg\ s^{-1}}}\right) \times \left(\frac{t_{var}}{1\ \mathrm{s}}\right)^{-2}\left(\frac{\bar{\Gamma}}{300}\right)^{-6}\left(\frac{B}{1000\,\mathrm{G}}\right)^{-4}\left(\frac{\Gamma_e}{10^4}\right)^{-5}. \tag{29}$$

The very large exponents which appears in (29) show that a small variation of the parameters can induce large changes in the relative importance of the synchrotron and inverse Compton processes. In practice, we find that α_{IC} is generally small in the early part of a burst but increases at later times essentially as a result of the reduction of the equipartition magnetic field in shocks at large distances from the source (see Section 3.1 below).

To be efficient, the emission process must also occur on a time-scale t_{em} shorter than the shell expansion time t_{ex} (equation 2). Using $r \sim ct_{var}\bar{\Gamma}^2$, this condition becomes

$$\frac{t_{syn}}{1+Q_{IC}} < \bar{\Gamma} t_{var}, \tag{30}$$

where $Q_{IC} = \tau_\star \Gamma_e^2$ (respectively $\tau_\star \Gamma_e^2/w$) for $w \ll 1$ (respectively $w \gg 1$). With expressions (11), (13), (14) and (20) above, (30) can be written

$$2\ 10^{-4}\alpha_B^{-1}(\Gamma_{int}-1)^{-1}\left(\frac{\dot{E}}{10^{52}\ \mathrm{erg\ s^{-1}}}\right)^{-1} \times\left(\frac{t_{var}}{1\ \mathrm{s}}\right)\left(\frac{\bar{\Gamma}}{300}\right)^5\left(\frac{\Gamma_e}{10^4}\right)^{-1} < 1+Q_{IC}. \tag{31}$$

This is more easily satisfied when gamma-rays directly come from synchrotron emission, since then $\Gamma_e \sim 10^4$. However, even for $\Gamma_e \sim 10^2$ the emission time remains smaller than the expansion time as long as the shocks are sufficiently strong ($\Gamma_1/\Gamma_2 \gtrsim 2$).

Some results of a model in which GRBs are produced by the inverse Compton process have been already presented elsewhere (Mochkovitch & Fuchs 1996). In this study we limit ourselves to synchrotron emission models except when we discuss the optical properties which strongly differ between the two cases. In synchrotron emission models the total efficiency for the conversion of wind kinetic energy to gamma-rays below a few MeV is given by

$$f_{tot} = f_d \times \alpha_e(1-\alpha_{IC}), \tag{32}$$

where α_e is the fraction of the dissipated energy which is transferred to the electrons. According to Bykov & Mészáros (1996), α_e is comparable to the fraction $\alpha_M \sim 0.1$–1 of the energy which is initially injected into magnetic fluctuations. The total efficiency therefore does not exceed a few per cent, which imposes severe constraints on the energy source or/and system geometry.

The energy available from disc accretion to a black hole

$$E \simeq \frac{1}{6}M_D c^2 = 3\times 10^{53}\left(\frac{M_D}{M_\odot}\right)\ \mathrm{erg}, \tag{33}$$

where M_D is the disc mass, can be less than 10^{53} erg for the coalescence of two neutron stars since numerical simulations indicate that $M_D \sim 0.2$–$0.3\ M_\odot$ (Rasio & Shapiro 1992; Davies et al. 1994; Ruffert, Janka & Schaefer 1996). The conversion of disc gravitational energy into wind kinetic energy should then be very efficient in order to account for cosmological GRBs. Naturally, if the wind is beamed in a solid angle $\delta\Omega$ along the system axis, the energy requirement is smaller by a factor $\delta\Omega/2\pi$ but one has now to face a statistical problem since even optimistic estimates of the neutron star merging rate are not considerably larger than the burst rate (Phinney 1991; Narayan, Piran & Shemi 1991; Tutukov & Yungelson 1993; Lipounov et al. 1995). The situation is less critical if the disc results from the disruption of a neutron star by a black hole or the collapse of a massive star, because the mass of the disc can be $M_D \gtrsim 1\ M_\odot$ (and even $M_D \gtrsim 10\ M_\odot$).

3 TEMPORAL PROPERTIES

3.1 Burst profiles

We first study the temporal properties of our burst models when the Lorentz factor in the wind has the simple shape shown in Fig. 1. We inject an energy $\dot{E} = 10^{52}/4\pi$ erg s^{-1} sr^{-1} which, for an efficiency of conversion into gamma-rays of a few per cent, yields a total energy $E \simeq 10^{51}/4\pi$ erg sr^{-1} for a burst lasting a few seconds. We obtain the burst profiles (in number of photons per second between 50 and 300 keV, which corresponds to BATSE bands 2 and 3) by adding the contributions of all the internal elementary shocks which occur during the expansion of the wind as explained in Section 2. For each shock we compute $\alpha_{syn} = 1-\alpha_{IC}$ (equation 27) where α_{IC} is the fraction of the energy which goes to inverse Compton photons, the equipartition magnetic field B_{eq} (equation 13 with $\alpha_B = 1/3$), the electron Lorentz factor Γ_e (equation 24 with $\alpha_M/\zeta = 1000$ and $\mu = 1.75$) and the synchrotron energy E_{syn} (equation 15). These quantities are represented in Fig. 3 as a function of arrival time t_a. As in Fig. 2, there are two branches corresponding to the forward and reverse shocks. Typical values are 10^2–10^4 G for the magnetic field, 2–20×10^3 for the electron Lorentz factor and 10 keV–1 MeV for the synchrotron energy.

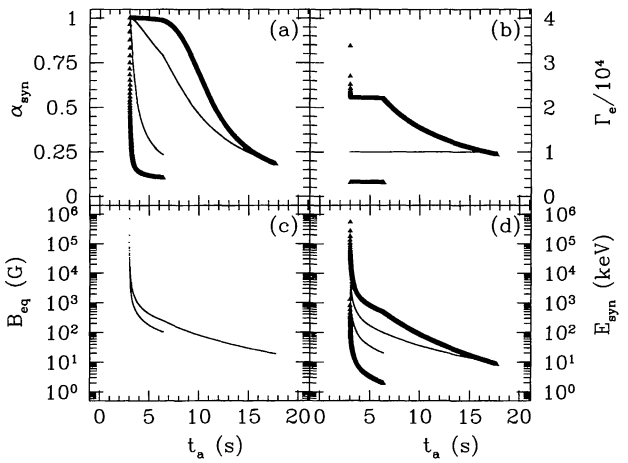

Figure 3. Physical parameters governing the emission mechanism: (a) fraction $\alpha_{syn} = 1-\alpha_{IC}$ of the energy which is radiated by the synchrotron process; (b) Lorentz factor Γ_e of the relativistic electrons; (c) equipartition magnetic field B_{eq}; (d) synchrotron energy E_{syn}. In (a), (b) and (d) the thick lines correspond to Γ_e given by equation (24) and the thin lines to $\Gamma_e = 10^4$.

The photons produced in the elementary shocks are distributed according to a synchrotron spectrum

$$\frac{dn(E)}{dE} \propto \frac{e}{E_{syn}}\left(\frac{E}{E_{syn}}\right)^{-x}, \tag{34}$$

with $x = 2/3$ for $E < E_{syn}$, $2 < x < 3$ for $E > E_{syn}$ and where e is the energy which is dissipated in the shock (equation 5). The resulting burst profile is shown in Fig. 4(a) for a high energy index $x = 2.5$. Cosmological effects (time dilation and redshift) have been taken into account, assuming that the burst is located at $z = 0.5$. The duration t_{90} which, according to the definition used for the BATSE data is the time during which 90 per cent of the total fluence is received (excluding the first and last 5 per cent) is 10.04 s, very similar to the duration of wind emission t_w. The decay after maximum is close to an exponential, as can be seen in the plot of the logarithm of the count rate versus time in Fig. 4(b) where there is a quasi-linear decline after maximum between $t \simeq 12$ and $t \simeq 20$ s. However, the rise time in our profile is not much shorter than the decay time and the burst is therefore not very dissymmetric if we except the low-intensity exponential tail after $t = 15$ s. We found that a profile much closer to the characteristic 'fast rise exponential decay' (FRED) shape observed in many bursts (or in individual pulses inside a complex burst) can be obtained by assuming that the

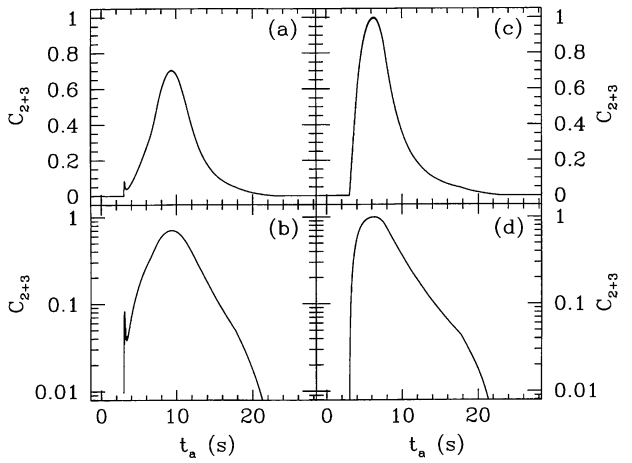

Figure 4. Burst profiles for the initial distribution of the Lorentz factor shown in Fig. 1. The count rate C_{2+3} (in arbitrary units) is given in the interval 50–300 keV, corresponding to BATSE bands 2 and 3; (a) profile obtained with equation (24) for the electron Lorentz factor; (b) same as (a) with C_{2+3} in logarithmic scale which illustrates the exponential decay after maximum; (c) profile obtained with a constant $\Gamma_e = 10^4$; (d) same as (c) with C_{2+3} in logarithmic scale.

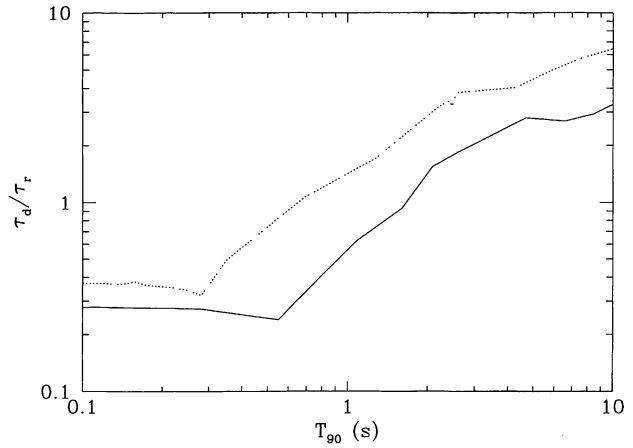

Figure 5. Solid line: ratio of the decay time to the rise time of burst profiles obtained with an initial distribution of the Lorentz factor homothetic to that shown in Fig. 1 but with different durations. For $t_{90} < 1.65$ s the profiles decay faster than they rise. Dashed line: the discontinuity in the initial distribution of the Lorentz factor has been replaced by a smoother transition (equation 36). Now, only bursts with $t_{90} < 0.65$ s decay faster than they rise.

electron Lorentz factor varies more slowly with ϵ (the dissipated energy per proton) than a power law of index $1/(3-\mu)$ (equation 24). This would be the case if the fraction ζ of accelerated electrons increased with ϵ. Such a behaviour is observed in simulations of collisionless non-relativistic shocks (Bykov, private communication) and we have supposed that it remains valid in the relativistic limit. Moreover, we have made the simple choice $\zeta \propto \epsilon$, which leads to a characteristic Lorentz factor for the electrons which is independent of ϵ. The synchrotron energy in the elementary shocks has been represented in Fig. 3(d) for a constant $\Gamma_e = 10^4$ and the corresponding burst profile is shown in Fig. 4(c). It now has a typical FRED shape with a ratio of the decay time to the rise time $\tau_d/\tau_r = 3.4$ where τ_r and τ_d are defined respectively by

$$\tau_r = t_{max} - t_5 \quad , \quad \tau_d = t_{95} - t_{max}, \tag{35}$$

where t_{max} is the time of maximum count rate and t_5 (respectively t_{95}) the time when 5 per cent (respectively 95 per cent) of the total fluence has been received.We have tested with our model the tendency for short bursts (or short pulses within a complex burst) to become more symmetric (Norris et al. 1996). We have computed the profiles obtained when the duration of wind emission t_w is varied while the initial distribution of the Lorentz factor remains homothetic to a given shape for which we choose the one represented in Fig. 1 where the wind consists of a slow part ($\Gamma = 100$) followed by a rapid part ($\Gamma = 400$) both containing the same mass. The results (for $z = 0.5$) are shown in Fig. 5 where we have plotted the ratio τ_d/τ_r as a function of t_{90}. It appears that τ_d/τ_r decreases from about 3 when $t_{90} \simeq 10$ s to about 0.3 when $t_{90} \lesssim 0.5$ s with $\tau_d/\tau_r = 1$ for $t_{90} \simeq 1.65$ s. We therefore reproduce the observed behaviour but the effect is even exaggerated for the shortest pulses, which decay faster than they rise. We believe that this might be a consequence of the crude assumptions made in our simple model and we expect that more detailed hydrodynamical simulations (Daigne & Mochkovitch, in preparation) could help to improve the profiles. Already we have found that better results can be obtained (with $\tau_d/\tau_r = 1$ for $t_{90} \simeq 0.65$ s) if the discontinuity between the two extreme values of Γ is replaced by a smoother transition of the form

$$\Gamma(t/t_w) = 250 + 150\cos[2.5\pi(t/t_w - 0.6)], \tag{36}$$

for $0.6 \leq t/t_w \leq 1$ and $\Gamma = 400$ for $t/t_w < 0.6$. However, the efficiency f_d of the dissipation process is then reduced by nearly a factor of 2.

Norris et al. (1996) have shown that in most cases complex bursts can be analysed in terms of a series of (possibly overlapping) pulses. In the same way we build complex bursts with our model by the addition of intensity pulses formed in the deceleration of rapid parts of the wind by slower ones which were emitted previously. We suppose that the initial distribution of the Lorentz factor is made of a rapid component (with an average value of Γ of a few hundreds) and of some slower layers (with $\Gamma \simeq 100$). The total mass in the slow layers has to be comparable to the mass in the rapid component in order to keep the efficiency at a reasonable level. A few examples of synthetic profiles are presented in Fig. 6. It can be seen that a great diversity of burst shapes can be obtained if the distribution of the Lorentz factor in the wind varies from one event to the other.

3.2 Short time-scale variability

The profiles shown in Figs 4 and 6 have a satisfactory general shape but do not exhibit any variability on a short time-scale. Rapid temporal variations cannot result from small irregularities of the emitting surface since photons coming from many different regions in space and time are received at a same time by the observer, which leads to a loss of coherence of the temporal variations (Woods & Loeb 1995; Sari & Piran 1997b,c). Instead, one has to consider again that the Lorentz factor itself can fluctuate at the millisecond level. This is not unrealistic if the flow at the origin of the wind is very irregular and turbulent since 1 ms corresponds to the typical dynamical time-scale of a disc orbiting a stellar mass black hole. As nothing is known about the temporal spectrum of the fluctuations, we have simply added a random fluctuation to the Lorentz factor of

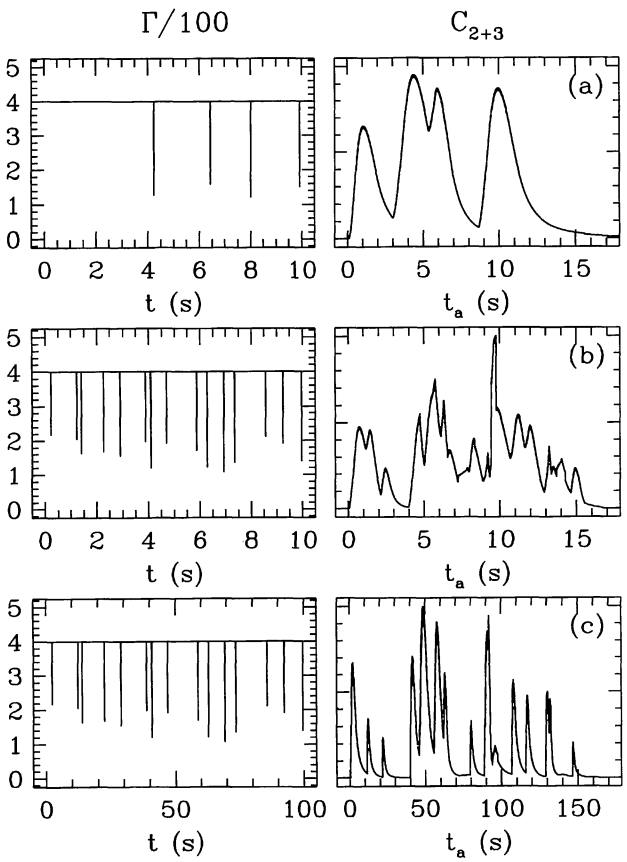

Figure 6. Burst profiles for three initial distributions of the Lorentz factor in the wind. In all three cases a rapid component with $\Gamma = 400$ is decelerated by a series of slower layers. The masses in the rapid component and slower layers are comparable. (a) Relatively simple profile with four layers which produce four intensity pulses, two of which partially overlap; (b) and (c) more complex profiles with 15 slow layers. Notice that the distributions of the Lorentz factor in (b) and (c) are homothetic, (c) being simply 10 times longer than (b).

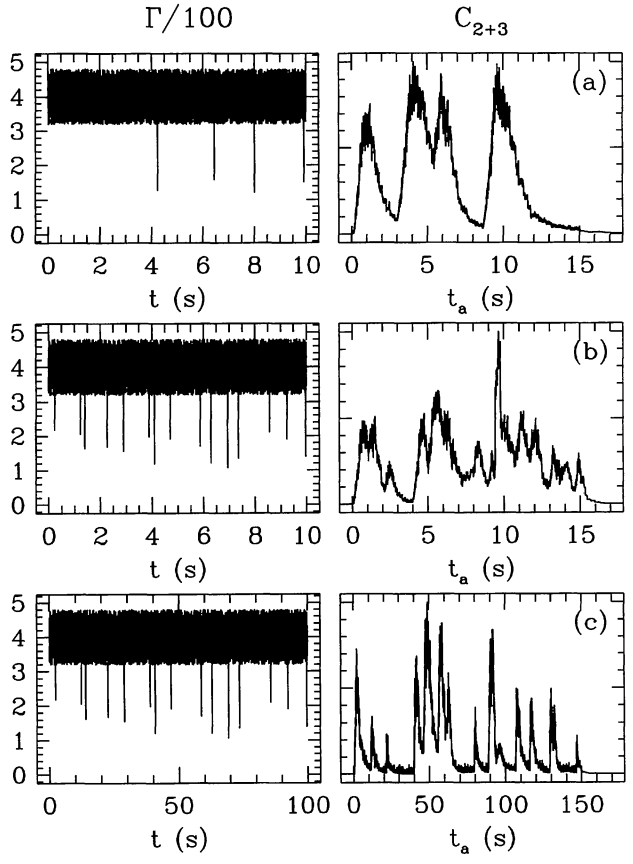

Figure 7. Same as Fig. 6 with a random fluctuation (of maximum amplitude ± 20 per cent) added to the average value $\Gamma = 400$ of the rapid component of the wind. The resulting profiles now exhibit variability on a short time-scale.

each of the layers initially injected (every 2 ms) in the wind. The adopted amplitude for these fluctuations is 10–20 per cent of the average value of Γ. The resulting profiles represented in Fig. 7 now show the rapid temporal variations which are seen in most observed bursts.

4 SPECTRAL PROPERTIES

4.1 Burst spectrum

The overall burst spectrum is the sum of all the elementary contributions (equation 34) from the internal shocks. The spectrum corresponding to the profile shown in Fig. 7(a) is represented in Fig. 8 (again a cosmological redshift $z = 0.5$ has been assumed). Its shape can be easily understood: let $E_{\rm syn}^{\rm min}$ and $E_{\rm syn}^{\rm max}$ be the minimum and maximum of the synchrotron energy for the whole set of elementary shocks. As long as E is smaller (respectively larger) than $E_{\rm syn}^{\rm min}$ (respectively $E_{\rm syn}^{\rm max}$) the number of photons $n(E)$ per unit energy interval is a power law of index −2/3 (respectively −2.5) and in the intermediate region the current index evolves from −2/3 to −2.5 as E goes beyond the value of $E_{\rm syn}$ for a growing number of elementary shocks. In the four BATSE bands, between 20 keV and a few MeV, the spectrum can be well described with Band's formula (Band et al. 1993)

$$n(E) = A\left(\frac{E}{100\ \text{keV}}\right)^{\alpha}\exp\left(-\frac{E}{E_0}\right) \quad \text{for} \quad (\alpha-\beta)E_0 \geq E,$$

$$n(E) = A\left[\frac{(\alpha-\beta)E_0}{100\ \text{keV}}\right]^{\alpha-\beta}\exp(\beta-\alpha)\left(\frac{E}{100\ \text{keV}}\right)^{\beta} \quad \text{for} \quad (\alpha-\beta)E_0 \leq E. \tag{37}$$

The parameters α, β and E_0 have been adjusted to obtain the best possible fit of the spectrum in Fig. 8. We get $\alpha = -1.33$, $\beta = -2.31$ and $E_0 = 544$ keV, in agreement with typical values found in observed bursts. The product $E^2n(E)$ is also shown in Fig. 8. It is at maximum at the peak energy $E_{\rm p} = 365$ keV, at which the bulk of the emission takes place.

4.2 Duration–hardness ratio relation

Shorter bursts are expected to be harder in our model. Internal shocks are formed at an approximate radius $r \sim ct_{\rm var}\bar{\Gamma}^2$ and are therefore closer to the source if the burst evolves on a short time-scale. Assuming that the injected power $\dot{E}$ is independent of the duration of wind injection $t_{\rm w}$, the equipartition magnetic field is stronger and the synchrotron energy is larger in the dissipation region for shorter bursts. To obtain the duration–hardness relation, we compute the hardness ratio $\rm HR_{32}$ (defined as the ratio of the number of photons received in BATSE band 3 to that in band 2) for bursts with homothetic initial distributions of the Lorentz factor but

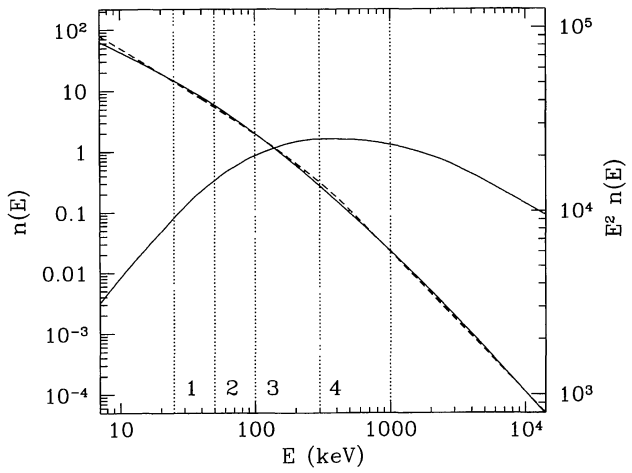

Figure 8. Spectrum of the burst corresponding to the profile of Fig. 7(a). The number of photons per energy interval $n(E)$ and the product $E^2n(E)$ are shown in arbitrary units. The dashed line is a fit of the spectrum with Band's formula in the interval 10 keV–10 MeV. The product $E^2n(E)$ is maximum at the peak energy $E_p = 365$ keV.

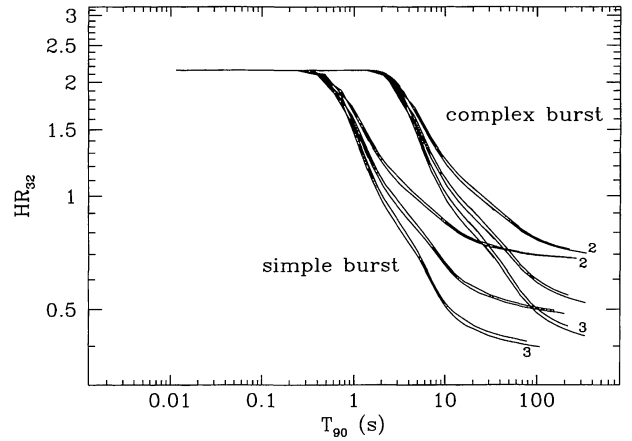

Figure 9. Duration–hardness ratio (HR_{32}) relations for a simple (one pulse) burst and a complex burst with five pulses. The relations are shown for three values of the high-energy index $x = 2$, 2.5 and 3 of the elementary synchrotron spectrum and two redshifts $z = 0.3$ and 1. It can be seen that the effect of the redshift is negligible.

different values of t_w. For a given duration t_{90} the hardness ratio is a function of the high-energy index of the elementary spectrum (equation 34) (the bursts becoming softer when x increases from 2 to 3), of the detailed history of the Lorentz factor and of the cosmological redshift z. Complex bursts tend to be harder because the distribution of the Lorentz factor varies on a shorter time-scale at given t_w and dissipation therefore begins earlier than in more regular bursts of the same duration. Finally cosmological effects shift bursts in the $HR_{32} - t_{90}$ diagram downward (redshift) and to the right (time dilation). However, the shift is nearly co-linear to the duration–hardness relation which therefore remains practically unchanged at different z. This is illustrated in Fig. 9 where the duration–hardness relation has been represented for several values of x and z and for a simple (single pulse) and a complex burst. In agreement with the observations (Kouveliotou et al. 1993; Dezalay et al. 1996) a transition occurs at $t_{90} \sim 2$ s. The shortest

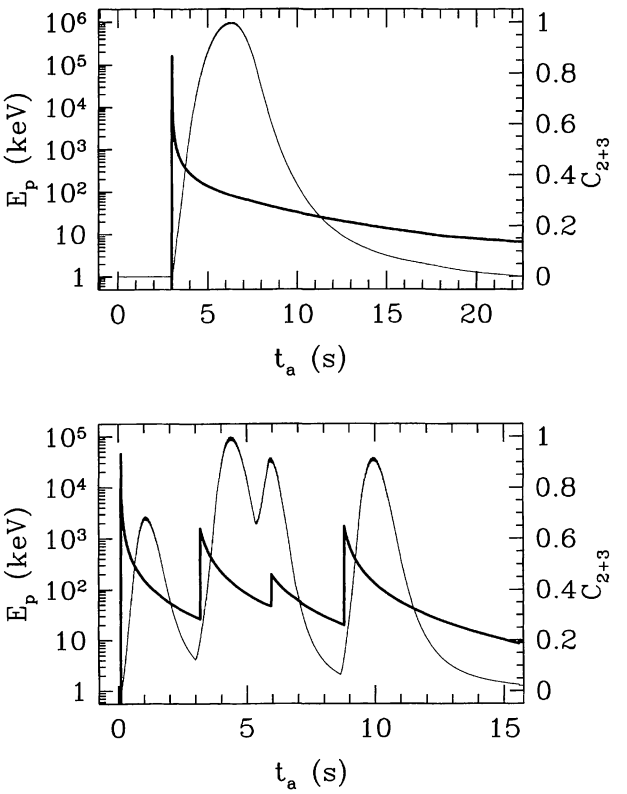

Figure 10. Evolution of hardness with time: the instantaneous value of the peak energy E_p (thick line) is represented together with the burst profile (thin line). Upper panel: for the simple one-pulse burst of Fig. 4(c). Lower panel: for the more complex burst of Fig. 6(a).

bursts reach a limit

$$HR_{32} \simeq \frac{300^{1/3} - 100^{1/3}}{100^{1/3} - 50^{1/3}} \simeq 2.1, \qquad (38)$$

when E_p is large enough for both BATSE bands 2 and 3 to lie in the region in which $n(E) \propto E^{-2/3}$. The longer bursts tend to various limiting values of the hardness ratio depending on the choice made for the high-energy index x.

4.3 Spectral evolution

4.3.1 Instantaneous hardness

The spectral evolution of GRBs shows a few trends which are followed by a majority of bursts, but also suffer some exceptions and are therefore not universal (Bhat et al. 1994; Ford et al. 1995). First, spectral hardness and count rate appear to be correlated. Within intensity pulses, both increase and decrease together, the hardness usually preceding the count rate. Another trend is a global hard-to-soft evolution over the course of the burst outside intensity pulses. Finally, later pulses, even if they have a greater intensity, tend to be softer than earlier pulses.

We have compared the spectral evolution of our synthetic burst models to these observational results. The hardness can be obtained as a function of time through the estimation of the instantaneous value of E_p, the energy of the peak of $E^2n(E)$. We first considered the simple burst of Fig. 4c which has a characteristic FRED shape and a duration $t_{90} = 10.23$ s. The hardness and count rate evolve similarly (see Fig. 10) but their maxima are separated by a time lag

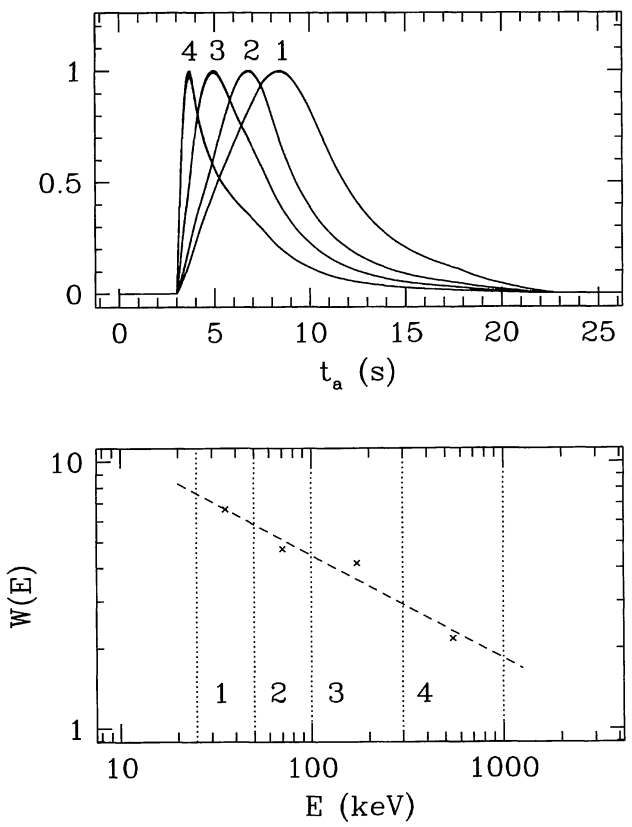

Figure 11. Upper panel: normalized profiles for the burst of Fig. 4(c) now represented in all four BATSE bands. Lower panel: half-maximum widths of the profiles as a function of energy. The fit of the model results (dashed line) has a slope $p = -0.39$.

of 0.89 s, the maximum of E_p occurring before that of the count rate. In complex bursts the hardness increases during intensity pulses and also precedes the count rate (Fig. 10).

The correlation between spectral hardness and count rate is therefore correctly reproduced in our models. We encountered more difficulties with the global hard-to-soft evolution which was observed in 70 per cent of the sample of bright long bursts studied by Ford et al. (1995). In synthetic bursts (Fig. 10) it is present as long as the profiles remain relatively simple (i.e. dominated by one main pulse or made of just a few pulses), while in complex bursts with many pulses only the correlation between hardness and count rate is clearly visible. Also, the hardness of successive pulses remains essentially correlated to the intensity, instead of decreasing as in 50 per cent of the Ford et al. (1995) sample.

4.3.2 Pulse shape as a function of energy

When observed in spectral bands of increasing energy, pulses become narrower, as shown by Norris et al. (1996) who analysed a large number of pulses in the four BATSE bands. They found that their (half-maximum) width can be well represented by a power law

$$W(E) \propto E^{-0.4}. \tag{39}$$

The same relation was obtained by Fenimore et al. (1995), who used the autocorrelation of averaged burst profiles instead of individual pulses. In our synthetic burst models the pulse width also decreases

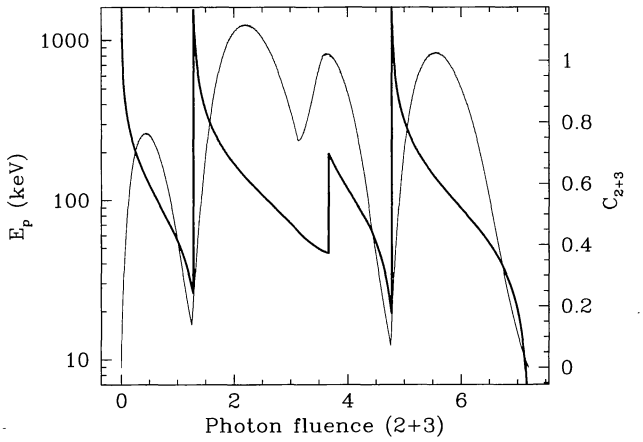

Figure 12. E_p–fluence relation (thick line) for the burst of Fig. 6(a). The peak energy is represented in logarithmic scale to show the section of linear decline following the moment of maximum count rate in the four intensity pulses. The photon fluence corresponds to the integrated photon flux in BATSE bands 2 and 3. The thin line shows the count rate in the same bands.

at high energy. Fig. 11 represents a single pulse burst in the four BATSE bands. The width can be fitted by power laws such as (39) but not with a unique exponent $p = -0.4$ for all the pulses. We indeed get $p \simeq -0.4$ for pulses of 2–10 s, but for pulses of 0.1–1 s, $p \gtrsim -0.2$. Norris et al. (1996) obtained $p = -0.4$ as an average on a collection of pulses with duration ranging from 0.1 to 10 s but do not provide the value of p for the shorter and longer pulses separately, which precludes a detailed comparison with our theoretical results.

4.4 The E_p–fluence relation

Liang & Kargatis (1996) discovered, in a sample of 37 BATSE bursts, an exponential dependence of the peak energy E_p on photon fluence F_{ph} during the declining part of intensity pulses, i.e.

$$E_p \propto \exp(-aF_{ph}). \tag{40}$$

The photon fluence is defined as the integral of the photon flux from the beginning of the burst, and a is the slope of the $\log E_p$–F_{ph} relation. In complex bursts the slope stays approximately constant from one pulse to another. Synthetic bursts also follow a relation such as (40), but the slope in successive pulses can vary somewhat, especially if the pulses have very different intensity or duration (see Fig. 12).

4.5 X-ray and optical counterparts

The X-ray and optical counterparts recently discovered in two GRBs have been interpreted in the context of cosmological models as the emission coming from a relativistic shell expanding in the interstellar medium (Wijers, Rees & Mészáros 1997; Vietri 1997; Waxman 1997a,b). If, however, GRBs are produced by internal shocks in a wind, X-ray to optical photons should also be emitted together with the gamma-rays before the afterglow resulting from the interaction with the interstellar medium.

To compute these early counterparts we consider a typical burst in which an energy $E = 2\ 10^{52}/4\pi$ erg sr^{-1} has been injected into the wind with a 5 per cent efficiency for the conversion to gamma-rays between 50 and 300 keV. For a GRB located at 2 Gpc ($z \sim 0.5$)

the observed fluence in BATSE bands 2 and 3 will be $F_\gamma \simeq 2\ 10^{-6}$ erg cm^{-2}. This value of F_γ is then used to normalize a synthetic spectrum from which the expected flux in the X-rays and visible can finally be obtained. In practice these fluxes are highly variable (as the gamma-rays) and have been averaged over the duration t_{90} of the burst.

We did not consider inverse Compton emission models in this paper, but we now briefly discuss their optical properties since they greatly differ from synchrotron emission models. When the gamma-rays come from inverse Compton scattering, a fraction $\alpha_{\rm syn} \sim 1 - \alpha_{\rm IC}$ of the total power is emitted at a typical synchrotron energy $E_{\rm p}/\Gamma_{\rm e}^2 \sim 10$–$100$ eV where $E_{\rm p}$ is the peak energy of the gamma-ray spectrum. The fraction $\alpha_{\rm syn}$ is fixed by the ratio $\alpha_{\rm e}/\alpha_{\rm B}$ through equations (17) and (23). Preliminary results indicate that for $\alpha_{\rm e}/\alpha_{\rm B} = 1$ the emission in the visible of a burst of fluence F_γ and duration $t_{90} = 10$ s could be as bright as $V = 5$–6 which is already excluded by the limit set by the ETC and GROCSE instruments (Krimm, Vanderspek & Ricker 1996; Lee et al. 1997). With $\alpha_{\rm e}/\alpha_{\rm B} = 100$ the predicted magnitude becomes $V = 8$–9, still within the reach of ETC and GROCSE.

In synchrotron emission models the optical counterpart is much weaker. Taking for example the spectrum represented in Fig. 8, which corresponds to a burst with $t_{90} = 10.55$ s, we get a V magnitude of 18.4 for $F_\gamma \simeq 2\times10^{-6}$ erg cm^{-2}. A larger fluence would naturally produce a brighter counterpart, possibly up to $V \sim 15$–16 for $F_\gamma \gtrsim 2\times10^{-5}$ erg cm^{-2}. An optical emission in this luminosity range should be detectable by the next generation of counterpart search instruments, such as the TAROT project (Boer 1997).

In X-rays the calculated fluxes for the BeppoSAX Wide Field Camera are in reasonable agreement with the observations. In the case of GRB 970228 the X- and gamma-ray fluences during the first 100 s are $F_{\rm X}(2-10\ {\rm keV}) \simeq 1.2\times10^{-6}$ and $F_\gamma(40-700\ {\rm keV}) \simeq 1.1\times10^{-5}$ erg cm^{-2} (Costa et al. 1997a). For the same gamma-ray fluence the model predicts $F_{\rm X}^{\rm model} \simeq 0.7$–$1.1\times10^{-6}$ erg cm^{-2} depending on burst hardness (the upper and lower limits of $F_{\rm X}^{\rm model}$ respectively correspond to bursts with $E_{\rm p} = 100$ and 350 keV).

In GRB 970508 the peak X-ray flux and the gamma-ray fluence are $\mathcal{F}_{\rm X}(2-10\ {\rm keV}) \simeq 1.2\times10^{-8}$ erg cm^{-2} s^{-1} and $F_\gamma(50$–$300\ {\rm keV}) \simeq 1.1\times10^{-6}$ erg cm^{-2} (Costa et al. 1997b; Kouveliotou et al. 1997). The calculated X-ray flux for a burst of comparable hardness, $\mathcal{F}_{\rm X}^{\rm model} \simeq 8\times10^{-9}$ erg cm^{-2} s^{-1}, is close to the observed value while the initial X-ray emission predicted by afterglow models appears to be an order of magnitude weaker (Sahu et al. 1997b). This can be considered as an indication that both the gamma-rays and the initial X-ray emission are produced by internal shocks.

The evolution of the afterglow which follows the emission from internal shocks can be obtained from a solution of the relativistic Sedov problem (Mészáros & Rees 1997b). Such a solution applies when the expanding shell of mass M has swept up a mass $M_{\rm ISM} \sim M/\Gamma$ in the interstellar medium which occurs after a deceleration time

$$t_{\rm dec} \simeq 180\ E_{52}^{1/3} n_1^{-1/3} \Gamma_2^{-8/3}\ {\rm s}, \tag{41}$$

where E_{52} is the shell energy in units of $10^{52}/4\pi$ erg sr^{-1}, n_1 is the density of the interstellar medium in atom cm^{-3} and $\Gamma_2 = \Gamma/100$. Most of the energy is radiated at the synchrotron frequency of the relativistic electrons

$$\nu_{\rm s} \simeq 3\ 10^{16} \alpha_{\rm e}^2 \alpha_{\rm B} E_{52}^{1/2} t_{\rm day}^{-3/2}\ {\rm Hz}, \tag{42}$$

where $\alpha_{\rm e}$ and $\alpha_{\rm B}$ are the fractions of the dissipated energy which go to the electrons and magnetic field respectively. The flux at the synchrotron frequency is given by (Waxman, 1997a,b)

$$\mathcal{F}_{\rm s} \simeq 6.5\ 10^{-26} \sqrt{n_1} \alpha_{\rm B} E_{52} D_{\rm Gpc}^{-2}\ {\rm erg\ cm^{-2}\ s^{-1}\ Hz^{-1}}, \tag{43}$$

and for $\nu > \nu_{\rm s}$ by

$$\mathcal{F}_\nu = \mathcal{F}_{\nu_{\rm s}} \left(\frac{\nu}{\nu_{\rm s}}\right)^{-\beta}, \tag{44}$$

where $\beta = q - 1/2$, q being the exponent of the power-law distribution of the accelerated electrons [$N(\Gamma_{\rm e}) \propto \Gamma_{\rm e}^{-q}$]. The flux in the visible decreases from a maximum $\mathcal{F}_{\rm V}^{\rm max} \simeq \mathcal{F}_{\rm s}$ following a power law of index $-3\beta/2$ the value of β ($\sim 0.6 - 0.8$) being obtained from the observations. For GRB 970508 a fit of the data also provides $\mathcal{F}_{\rm V}^{\rm max} \simeq 6\ 10^{-28}$ erg cm^{-2} s^{-1} Hz^{-1} (Sahu et al. 1997b). With the gamma-ray fluence measured for this burst, and assuming a 5 per cent efficiency for the conversion of wind kinetic energy to gamma-rays, we obtain

$$\sqrt{n_1} \alpha_{\rm B} \simeq 3\ 10^{-2}. \tag{45}$$

If we adopt this value as typical we find that the afterglow of the burst (given in example above) with $E_{52} = 2$ and $D_{\rm Gpc} = 2$ has a V magnitude of 18.9 before the phase of power-law decline. In inverse Compton emission models the initial optical counterpart produced by internal shocks is considerably brighter than the afterglow, but in synchrotron emission models the two contributions have comparable brightness. However, the optical signal will present a short interruption if the duration of the burst is smaller than the deceleration time. Conversely, if $t_{\rm w} \gtrsim t_{\rm dec}$ the two contributions overlap and form a continuous signal. In any case, a detailed photometric follow-up in the optical range beginning before the end of the gamma-ray burst would certainly provide crucial information about the emission mechanisms.

5 CONCLUSIONS

We have developed a simple model in order to compute the temporal and spectral properties of GRBs under the assumption that they originate from internal shocks in a relativistic wind. We have not discussed the critical point of how such a wind could form, but the recent observations of optical counterparts for GRB 970228 and GRB 970508 seem to indicate that a relativistic shell was indeed present in these objects.

The distribution of the Lorentz factor in the wind has no reason to be uniform and variations on several time-scales (down to 1 ms which corresponds to the dynamical time-scale of a relativistic disc orbiting a stellar-mass black hole) can be expected. Layers of different velocities will collide and form internal shocks within the relativistic wind and the energy dissipated in these shocks can be emitted in the form of gamma-rays. We have followed the evolution of the relativistic wind using an approach where all pressure waves are suppressed so that layers only interact through direct shocks. We assume that the magnetic field reaches equipartition in these shocks and that the electron Lorentz factor remains close to a constant value $\Gamma_{\rm e} \sim 10^4$. This could be the case if, according to Bykov & Mészáros (1996), only a small fraction ζ of the electrons is accelerated in the shocks and if ζ is also approximately proportional to the dissipated energy. Gamma-rays are then directly produced by synchrotron emission from the relativistic electrons.

This procedure allows us to construct synthetic bursts, the temporal and spectral properties of which are compared to the observations. We obtain a series of encouraging results.

(1) It is possible to generate a great diversity of profiles simply by playing with the initial distribution of the Lorentz factor in the wind.

(2) The profile of individual pulses is asymmetric, close to a 'FRED' shape.

(3) The short time-scale variability of the profiles can be explained if the Lorentz factor itself varies at the millisecond level.

(4) Synthetic spectra can be fitted with Band's formula with parameters α, β and E_0 comparable to those of observed bursts.

(5) The duration–hardness relation is a natural consequence of the model, since in short bursts dissipation occurs closer to the source where the magnetic field and the synchrotron energy are larger.

(6) Spectral hardness and count rate are correlated during burst evolution, the hardness generally preceding the count rate.

(7) The pulse width decreases with increasing energy following a power law $W(E) \propto E^{-p}$ with $p \sim 0.4$ for pulses of duration 2–10 s.

(8) In the declining part of intensity pulses, the peak energy E_p decreases exponentially with photon fluence.

Some other properties of observed GRBs are, however, not so well reproduced by our model.

(1) The shortest pulses tend to decay faster than they rise instead of being symmetric.

(2) Synthetic bursts do not show a global hard-to-soft evolution as frequently as real bursts.

(3) The slope of the E_p–fluence relation can differ among pulses inside the same burst.

It is not yet clear whether these difficulties represent real problems for our model or are simply a consequence of some of the crude assumptions we have made. In particular, the evolution of the wind should be followed with a detailed hydrodynamical code (Daigne & Mochkovitch, in preparation) rather than with the simple method used here.

A more fundamental issue may be the rather low efficiency for the conversion of wind kinetic energy to gamma-rays. If GRBs result from the coalescence of neutron stars the wind cannot be strongly beamed, since the merging rate is not very much greater than the burst rate. A large fraction of the energy released in the coalescence should therefore be injected into the wind.

We believe that the present work has shown that if a relativistic wind carrying enough energy can be produced, the internal shock model appears as a convincing candidate to explain GRBs. Ways to both reach a high efficiency in the generation of the wind and to avoid at the same time baryonic pollution are among the difficult problems that remain to be solved.

REFERENCES

Band D. et al., 1993, ApJ, 413, 281
Baring M. G., 1995, Ap&SS, 231, 169
Bhat P. N., Fishman G. J., Meegan C. A., Wilson R. B., Kouveliotou C., Paciesas W. S., Pendleton G. N., Schaeffer B. E., 1994, ApJ, 426, 604
Blandford R. D., Znajek R., 1977, MNRAS, 179, 433
Boer M., 1997, in Rencontres de Moriond 'Very High Energy Phenomena in the Universe', in press
Bykov A., Mészáros P., 1996, ApJ, 461, L37
Costa E. et al., 1997a, Nat, 387, 783
Costa E. et al., 1997b, IAU Circ. No. 6649
Davies M. B., Benz W., Piran T., Thielemann F. K., 1994, ApJ, 431, 742
Dezalay J. P., Lestrade J. P., Barat C., Talon R., Sunyaev R., Terekhov O., Kuznetsov A., 1996, ApJ, 471, L27
Eichler D., Livio M., Piran T., Schramm D., 1989, Nat, 340, 126
Fenimore E. et al., 1993, Nat, 366, 40
Fenimore E. et al., 1995, ApJ, 448, L101
Fenimore E., Madras C., Nayakshin S., 1997, ApJ, 473, 998
Fishman G. J., Meegan C. A., 1995, ARA&A, 33, 415
Ford L. A. et al., 1995, ApJ, 439, 307
Hartmann D. H., Brown L. E., The L. S., Linder E. V., Petrosian V., Blumenthal G. R., Hurley K., 1994, ApJS, 90, 893
Kobayashi S., Piran T., Sari R., 1997, ApJ, 490, 92
Kouveliotou C., Meegan C. A., Fishman G. J., Bhat N. P., Briggs M. S., Koshut T. M., Paciesas W. S., Pendleton G. N., 1993, ApJ, 413, L101
Kouveliotou C. et al., 1997, IAU Circ. No. 6660
Krimm H. A., Vanderspek R. K., Ricker G. R., 1996, A&AS, 120, 251
Lee B. et al., 1997, ApJ, 482, L125
Liang E., Kargatis V., 1996, Nat, 381, 49
Lipunov V. M., Postnov K. A., Prokhorov M. E., Panchenko I. E., Jorgensen H. E., 1995, ApJ, 454, 593
Mao S., Paczyński B., 1992, ApJ, 388, L45
Mészáros P., Rees M. J., 1992, MNRAS, 257, 29
Mészáros P., Rees M. J., 1993, ApJ, 405, 278
Mészáros P., Rees M. J., 1997a, ApJ, 482, L29
Mészáros P., Rees M. J., 1997b, ApJ, 476, 232
Mészáros P., Laguna P., Rees M. J., 1993, ApJ, 415, 181
Metzger M. R., Djorgovski S. G., Kulkarni S. R., Steidel C. C., Adelberger K. L., Frail D. A., Costa E., Frontera F., 1997, Nat, 387, 878
Mochkovitch R., Fuchs Y., 1996, in Kouveliotou C., Briggs M. F., Fishman G. J., eds, AIP Conf. Proc. 384, 3rd Huntsville Symp. on Gamma-Ray Bursts. Am. Inst. Phys., New York, p. 772
Mochkovitch R., Hernanz M., Isern J., Martin X., 1993, Nat, 361, 236
Mochkovitch R., Hernanz M., Isern J., Loiseau S., 1995, A&A, 293, 803
Narayan R., Piran T., Shemi A., 1991, ApJ, 379, L17
Narayan R., Paczyński B., Piran T., 1992, ApJ, 395, L83
Nemiroff R. J., 1995, The 75th Anniversary Astronomical Debate on the Distance Scale to Gamma-Ray Bursts, PASP, 107, 1131
Norris J. P., Nemiroff R. J., Bonell J. T., Scargle J. D., Kouveliotou C., Paciesas W. S., Meegan C. A., Fishman G. J., 1996, ApJ, 459, 393
Paczyński B., 1991, Acta Astron., 41, 257
Paczyński B., Xu G., 1994, ApJ, 427, 708
Panaitescu A., Mészáros P., 1997, preprint astro-ph/9703187
Panaitescu A., Wen L., Laguna P., Mészáros P., 1997, ApJ, 482, 942
Papathanassiou H., Mészáros P., 1996, ApJ, 471, L91
Phinney E. S., 1991, ApJ, 380, L17
Piran T., 1992, ApJ, 389, L45
Rasio F. A., Shapiro S. L., 1992, ApJ, 401, 226
Rees M. J., Mészáros P., 1992, MNRAS, 258, 41P
Rees M. J., Mészáros P., 1994, ApJ, 430, L93
Ruffert M., Janka H. T., Schaefer G., 1996, A&A, 311, 532
Ruffert M., Janka H. T., Takahashi K., Schaefer G., 1997, A&A, 319, 122
Sahu K. C. et al., 1997a, Nat, 387, 479
Sahu K. C. et al., 1997b, ApJ, 489, L127
Sari R., Piran T., 1997a, MNRAS, 287, 110
Sari R., Piran T., 1997b, ApJ, 485, 270
Sari R., Piran T., 1997c, preprint astro-ph/9702093
Shaviv N. J., Dar A., 1995, MNRAS, 277, 287
Shaviv N. J., Dar A., 1996, preprint astro-ph/9608135
Shemi A., 1994, MNRAS, 269, 1112

Thompson C., 1994, MNRAS, 270, 480
Tutukov A. V., Yungelson L. R., 1993, MNRAS, 260, 675
van Paradijs J. et al., 1997, Nat, 386, 686
Vietri M., 1997, ApJ, 488, L105
Waxman E., 1997a, ApJ, 485, L5
Waxman E., 1997b, ApJ, 489, L33
Wijers R. A. M. J., Rees M. J., Mészáros P., 1997, MNRAS, 288, L51
Woods E., Loeb A., 1995, ApJ, 453, 583
Woosley S. E., 1993, ApJ, 405, 273

This paper has been typeset from a TEX/LATEX file prepared by the author.